NASA TECHNICAL NOTE

NASA TN D-4985

NASA TN D-4985

ANALYSIS OF NONEQUILIBRIUM AIR STREAMS IN THE AMES 1-FOOT SHOCK TUNNEL

by Robert S. Hiers, Jr., and John O. Reller, Jr.

Ames Research Center
Moffett Field, Calif.

NATIONAL AERONAUTICS AND SPACE ADMINISTRATION • WASHINGTON, D. C. • JANUARY 1969

NASA TN D-4985

ANALYSIS OF NONEQUILIBRIUM AIR STREAMS IN THE AMES 1-FOOT SHOCK TUNNEL

By Robert S. Hiers, Jr., and John O. Reller, Jr.

Ames Research Center
Moffett Field, Calif.

NATIONAL AERONAUTICS AND SPACE ADMINISTRATION

For sale by the Clearinghouse for Federal Scientific and Technical Information
Springfield, Virginia 22151 – CFSTI price $3.00

TABLE OF CONTENTS

	Page
SUMMARY	1
INTRODUCTION	1
LIST OF SYMBOLS	2
FACILITY	3
INSTRUMENTATION	4
Driven Tube	4
Test Section	5
EXPERIMENTAL RESULTS	7
Reservoir Conditions	7
Test Section Conditions	8
ANALYSIS OF RESULTS	10
Flow Models	10
Data Analysis	11
CONCLUDING REMARKS	12
APPENDIX A - SEMIEMPIRICAL SUDDEN-FREEZE MODEL	13
APPENDIX B - INFLUENCE OF CONTAMINATION ON STREAM CALIBRATION	15
REFERENCES	16
TABLES	18
FIGURES	21

ANALYSIS OF NONEQUILIBRIUM AIR STREAMS IN THE AMES 1-FOOT SHOCK TUNNEL

By Robert S. Hiers, Jr., and John O. Reller, Jr.

Ames Research Center

SUMMARY

An analysis and the results of a preliminary calibration of nonequilibrium test streams in the Ames 1-foot shock tunnel are presented. The facility is combustion driven and is normally operated in the tailored-interface mode to provide a nominal reservoir enthalpy of 9,100 J/gm and pressure of 275 atm. In addition, the shock tunnel is operated in the equilibrium-interface mode to provide enthalpies between 6,000 J/gm and 15,000 J/gm at a nominal reservoir pressure of 275 atm. Results are presented for three typical operating conditions.

Static pressure, pitot pressure, velocity, mass flow, and stagnation-point heat transfer were measured in the test stream. These data are compared with numerically integrated and sudden-freeze models for air undergoing both chemical and vibrational relaxation. It is shown that the sudden-freeze model is satisfactory for calibrating the test stream if certain frozen-flow parameters are determined using experimental data. An added advantage of this approach is that flow properties in the test stream may be obtained without specifying the relaxation rates.

The test durations are limited not by variations in reservoir pressure but by contamination of the test gas with driver gas.

INTRODUCTION

The 1-foot shock tunnel at the Ames Research Center is a hypervelocity testing facility suitable for both hypersonic flight simulation and basic aerodynamic studies. The facility is combustion driven and generates hypervelocity air flows for a range of reservoir enthalpies between 6,000 J/gm and 15,000 J/gm. In addition, hypersonic test streams of planetary gases such as carbon dioxide-nitrogen mixtures can also be generated.

The 1-foot shock tunnel develops a high-pressure gas reservoir for an unusually long duration by utilizing a large volume driver. (The design method is given in ref. 1.) As a result, the reservoir pressure remains relatively constant for several hundred milliseconds; however, reference 2 showed that the useful test duration is much shorter than this because of the limit imposed by the mixing of the driver gas with the test gas. Thus, the virtue

of the large-volume driver is only partly realized in the present application, and can be effectively utilized only when interface mixing is retarded.

The test streams generated in this facility are influenced by chemical and vibrational nonequilibrium. The calibration of these nonequilibrium test streams involves making certain measurements in the test stream and correlating these measurements with theoretical models of the flow to obtain other flow parameters such as Mach number, density, and area ratio.

The purpose of this investigation was to make a preliminary aerodynamic and thermodynamic calibration of nonequilibrium airflows in the Ames 1-foot shock tunnel. Five free-stream parameters were measured: static pressure, pitot pressure, mass flow, velocity, and stagnation-point heating rate. These measurements are compared with the corresponding variables obtained from streamwise integrations of the rate processes and from sudden-freeze calculations to determine the other properties of the test streams.

LIST OF SYMBOLS

$\frac{A}{A^*}$	effective nozzle area ratio, $\frac{\rho^* u^*}{\rho u}$
h	enthalpy, J/gm
M	Mach number
p	pressure, atm
$\dot{q}$	heating rate, W/cm^2
R	gas constant, 1.987 cal/mole - $^{\circ}K$
Re	Reynolds number, 1/cm
$\frac{S}{R}$	dimensionless entropy
t	time, msec
Δt	time required for fluid element to traverse nozzle
T	temperature, $^{\circ}K$
u	stream velocity
V_s	shock velocity
x	axial coordinate of driven tube, m
ρ	density, g/cm^2
$( )^*$	sonic conditions at nozzle throat

Subscripts

f	equilibrium value at freeze point
i	initial loading condition in driven tube
max	maximum value obtainable in steady, equilibrium expansion
p	value obtained from a mass flow probe
r	value behind reflected shock wave
t	isentropic stagnation condition in nozzle
t_2	stagnation condition behind normal shock wave on test-section probe

When used without subscripts p, ρ, T, u, A, and M denote static free-stream quantities.

FACILITY

The major components of the Ames 1-foot shock tunnel are shown schematically in figure 1. A large volume driver provides performance capability in the mode of operation described as the one-cycle shock compression process (ref. 1). In this mode of operation the pressure behind the reflected shock (reservoir pressure) remains essentially constant for several tenths of a second when the initial conditions in the driven tube are suitably chosen to provide a tailored interface (no wave reflections from the interface). The 1-foot shock tunnel is also operated in the equilibrium-interface mode, that is, with one or more wave reflections from the interface, by varying the initial conditions in the driven tube (ref. 3). Relatively small variations of reservoir pressure occur in the equilibrium-interface mode after the initial unsteady transient. Further details of the shock-tube operation are given in reference 2.

For operation, the driver is initially charged with a room-temperature mixture consisting of 7 percent H_2, 12 percent O_2, and 81 percent He by partial pressures. Final driver pressures of approximately 340 atm are normally obtained after combustion. The temperature of the combustion products in the driver is estimated to be 2080° K. Combustion durations between 500 and 800 msec are usually obtained. Diaphragm opening is initiated with a punch mechanism activated at a preset time after the combustion pressure reaches a maximum. Further details are given in reference 4.

For these tests, the driven tube was charged with dry air at room temperature to pressures of 0.54, 0.34, and 0.25 atm to generate reservoir enthalpies of 7,600, 9,100, and 10,900 J/gm at a nominal pressure of 275 atm. The corresponding reservoir temperatures are 4,950, 5,650 and $6,300^{\circ}$ K. The 0.34 atm loading condition results in nominal tailored-interface operation.

The end wall of the driven tube is as close to planar as conditions permit, to minimize disturbances when the incident shock wave is reflected. It was necessary to introduce a short inlet section, about 1.5 cm long, upstream of the sonic throat to avoid excessive heating and erosion of the throat during the relatively long test flow times (25 to 30 msec). Heat-sink cooling of the throat region is achieved with a large copper insert (see fig. 1). To prevent model damage from overheating, the flow is terminated at a preselected time by a squib-operated slide valve downstream of the throat. A nominal throat diameter of 0.5 cm was used for these tests.

The nozzle is conical and exhausts into a square test section. The test section is mechanically isolated from the nozzle by a slip joint that reduces the transmitted force acceleration below ±25 g, or about an order of magnitude less than that experienced by the driven tube and nozzle.

Before each test, the test section is isolated from the driven tube by a small plastic diaphragm placed over the nozzle entrance, and then is evacuated to about 10μ Hg to facilitate nozzle starting. The small diaphragm disintegrates and is swept from the test section during the nozzle starting process, which is of the order of 1 msec.

The calibration measurements were obtained on the nozzle centerline in the square test section at a location just downstream of the conical nozzle exit. The flow at this location is conical and well within the test rhombus, that is, it has not been influenced by the compression corner between the nozzle and the test section.

INSTRUMENTATION

Driven Tube

Pressure.- Side wall pressures were measured at several axial locations in the driven tube with flush-mounted quartz-crystal transducers.[1] These gages were used to measure pressure behind both the incident and reflected shock waves as well as the subsequent time variation of pressure. One gage was mounted about 2 cm from the reservoir end wall to measure the reservoir pressure as a function of time.

The output of the transducers was filtered with 50-kc low-pass filters to mask the initial gage acceleration response to the suddenly applied pressure load. Otherwise, these gages were relatively insensitive to the mechanical acceleration encountered during the tests. A thin layer of silicone rubber deposited on the diaphragm effectively insulated the gage from the thermal environment behind the shock waves. Additional details of the use of these gages are given in reference 2. The accuracy of the reservoir pressure measurements is ±2 percent.

---

[1]Kistler Instrument Corp. Model No. 601 H.

Shock wave velocity.- The velocity of the primary shock wave was determined as a function of axial distance in the driven tube by measuring the time of arrival of the shock wave at several stations with ionization probes. The probes have two closely spaced electrodes that are differentially biased (90 volts) prior to a test. Ionization behind the shock wave causes a current to flow between the electrodes; probe signals are recorded on microsecond counters. The overall error in measurement of shock velocity is less than 1 percent.

Test Section

Static pressure.- The static pressure was measured with a 1.27-cm-diameter cylindrical probe (fig. 2(a)). The forebody of the probe consists of a circular ogive with a 6-to-1 fineness ratio. The pressure is sensed by a variable-capacitance cell located in a small cavity immediately behind the multiple orifices. This cell was designed and constructed at the Ames Research Center; it employs a 0.0013 cm thick stretched diaphragm and is matched to a 100-kc carrier-amplifier system. The cell is insulated from thermal effects by several layers of very fine mesh copper screens located in the cavity. The nominal rated pressure is 4×10^{-4} atm, and the linear operating range is about a factor of 4 greater. The performance characteristics and associated circuitry of this type of cell are described further in reference 5.

The orifices are located on the probe afterbody, where perfect-gas characteristics solutions indicate the inviscid surface pressure is about 95 percent of the local free-stream value. Use of perfect-gas solutions is justified by the assumption that the flow about the probe is essentially frozen at the stream conditions, where the specific heat ratio is close to 1.40. It is estimated that boundary-layer displacement thickness effects cause about a 5-percent increase in local surface pressure over the calculated inviscid pressure at the orifice. Hence the inviscid overexpansion and the viscous effects on the probe pressure are approximately compensating. Orifice corrections were calculated and found to be negligible. The error in pressure measurements, including all effects, is estimated to be less than ± 7 percent.

The initial response time of this probe is dominated by the cavity filling time and is less than 2 msec. After this initial transient, the probe response time is estimated to be less than 0.5 msec.

Pitot pressure.- The pitot pressure in the free stream is measured with a flat-faced cylindrical probe (fig. 2(b)). The inviscid flow between the bow shock wave and the stagnation point on the pitot probe undergoes nonequilibrium chemical and vibrational relaxation. For the conditions of this test, the pitot pressure varies a maximum of 4 percent, depending on the degree of nonequilibrium behind the bow shock wave.

The pitot pressure is detected with a capacitance cell similar to that used to detect static pressure. The cell is positioned in a cavity behind the orifice and is also protected from the thermal environment with several layers of screens. The nominal rated pressure is 3×10^{-2} atm, the linear range is about a factor of 5 greater, and the accuracy of the pressure measurements

is within ±3 percent. The response time for this probe is estimated to be less than 0.5 msec.

Mass-flow rate.- The mass-flow rate per unit area was measured with the probe shown schematically in figure 2(c). The probe entrains the flow in a known cross-section area of the free stream. The flow in this stream tube is cooled to about room temperature inside the probe, then essentially stagnated. The flow is then expanded out of the probe through a calibrated sonic throat. The temperature and pressure of the essentially stagnated gas inside the probe are measured, and the mass-flow rate out of the calibrated sonic throat is calculated by means of the following perfect gas relationship, $\rho u \propto P_p/\sqrt{T_p}$. A comprehensive report of the design and use of such a probe is presented in reference 6.

The stagnation pressure inside the probe is measured with two variable-inductance cells rated at 0.14 atm but having a linear range several times this value. The stagnation temperature is measured with a number 40-gage chromel-constantan thermocouple located in the stagnation chamber. The overall accuracy of mass-flow measurements is estimated to be within ±5 percent.

Approximately 8 msec are initially required to fill the mass-flow probe and establish steady-state operation; after this transient the response time of the probe is about 2 msec.

Free-stream velocity.- The free-stream velocity was measured, with the twin-rail probe shown in figure 2(d), by determining the distance a column of ionized gas travels in a known time interval.

The column of ionized gas is formed by generating a very short duration current discharge (~3 μsec) of known pulse shape between the two tip electrodes, after supersonic flow has been established in the nozzle. The resulting column of ionized gas is swept downstream between the rails. At a predetermined time after the tip electrodes have discharged (~35 μsec), the rail electrodes are discharged through the same ionized column. These two discharges provide one velocity measurement. The pulse-generating equipment can discharge three such spark pairs during a test, thus providing three measures of velocity in a minimum elapsed time of 10 msec. Analysis and measurement of electrical parameters in the pulse circuits indicated the energy into each spark to be less than 0.04 joule. According to the study of reference 7, energy of this magnitude should cause a temperature rise of only a few degrees in the spark column; thus there should not be any appreciable thermal expansion of the column to detract from the accuracy of measurement.

The column of ionized gas is luminous during each discharge and its position is recorded photographically. The distance between the two peak luminosities is measured with a microdensitometer and is assumed to be the distance traversed by a fluid element in the free stream. The error is estimated to be about ±3 percent. This technique is discussed in considerable detail in reference 7.

Stagnation-point heat transfer.- The transient heating technique described in reference 8 was used to measure the stagnation-point heat-transfer rates on a 2.5-cm diameter copper hemisphere.

The skin thickness of the copper hemisphere was approximately 0.025 cm. A thermocouple junction was formed at the stagnation point by inserting number 40-gage chromel constantan thermocouple wires into two holes, 0.13 mm in diameter, approximately 0.75 mm apart. The clearance between the wires and holes is filled with high-temperature solder to complete the junction.

Wire conduction and lateral skin conduction errors are negligible for the time scale of these tests. The measurement error is estimated to be less than 5 percent. The thermal response time of the model skin - the time required for the probe to indicate the appropriate quasi-steady heating rate - is less than 1/2 msec.

EXPERIMENTAL RESULTS

The experimental results obtained for one of the three test conditions considered in this report are presented in this section. These results are typical of the basic data for each of the three test conditions and illustrate various features of the flow. The Analysis of Results section summarizes the experimental data for all three test conditions and compares them with theoretical models of the flow to establish the aerodynamic calibration of the test stream at each of the three reservoir states.

Reservoir Conditions

The initial reservoir pressure and enthalpy are found as a function of the driven-tube loading conditions and the measured shock wave velocity by solving for conditions behind the reflected shock wave. The thermodynamic properties behind the incident and reflected shock waves are in local equilibrium because of the relatively high-density conditions in the driven tube. The velocity of the incident shock wave is shown as a function of axial distance in the driven tube in figure 3 for the nominal tailored-interface conditions (p_i = 0.34 atm). As indicated, the shock wave does not attenuate appreciably; hence the appropriate velocity is determined with little uncertainty.

The subsequent time variation of reservoir pressure for p_i = 0.34 atm is shown in figure 4(a). The initial calculated reservoir pressure (that of the reflected shock) is also indicated. Note that the initial reservoir pressure is not accurately resolved in these data; that is, the response of the recording oscillograph was not sufficient to provide an accurate indication of pressure for the first 1 to 2 msec after shock arrival. However, oscilloscope data (ref. 2) for this case show that the measured and calculated initial reservoir pressure agree well. Figure 4(a) also indicates that a slightly overtailored condition was obtained, as evidenced by the slight drop in pressure below p_r for several milliseconds. The gradually rising

pressure that follows is attributed to a secondary wave system originating at the conical transition inlet to the shock tube, as discussed in reference 2.

The variation of reservoir enthalpy with time is calculated by assuming that the reservoir entropy is constant at its initial value behind the reflected shock wave, while the reservoir pressure corresponds to its experimental value. Shock-tube performance calculations in reference 2 indicate that this assumption is essentially exact for the cases considered here. The resulting reservoir enthalpy for $p_i = 0.34$ atm is shown in figure 4(b). Also shown is the initial reservoir enthalpy, based on the initial entropy and the initial calculated pressure.

The stagnation-point heat-transfer rate measured on the test-section centerline for $p_i = 0.34$ atm is shown in figure 5 to substantiate the method used to calculate the reservoir enthalpy. The heat-transfer rate calculated by the method of Fay and Riddell (ref. 9), using the measured stagnation-point pressure and the calculated reservoir enthalpy, is also shown. The theoretical curve represents the limit for an equilibrium boundary layer. Following reference 9, this heating rate should be nearly the same regardless of the state of the boundary layer, since the surface material (copper) is relatively catalytic to recombination. The good agreement obtained between the measured and calculated heat-transfer rates indicates that the calculated enthalpy in figure 4(b) is substantially correct.

The time-dependent reservoir properties, pressure and enthalpy (figs. 4(a) and (b)), can be related instant by instant to local free-stream conditions in the nozzle if the quantities $(dp_t/dt)(\Delta t/p_t)$ and $(dh_t/dt)(\Delta t/h_t)$ are small compared to unity, where Δt is the time required for a fluid element to traverse the nozzle. In fact, these quantities are less than 0.02 in magnitude. Thus, although the reservoir pressure and enthalpy are functions of time, they can be considered quasi-steady with respect to free-stream conditions since their variation is negligible for time increments of the order required for a fluid element to traverse the nozzle, $\Delta t \approx 0.3$ msec.

Reservoir properties for the other operating conditions considered in this report ($p_i = 0.25$ atm and 0.54 atm) were determined in a manner similar to that described for $p_i = 0.34$ atm.

Test-Section Conditions

Static pressure.- A static-pressure history for $p_i = 0.34$ atm, normalized by the reservoir pressure, is shown in figure 6(a). After the initial probe and nozzle transients have occurred, the static-pressure ratio is essentially constant for a time interval of approximately 12 msec, as shown by the filled symbols on the figure. Hence the nozzle and reservoir are operating in a quasi-steady manner during this period, as expected.

However, after 12 msec have elapsed, the static pressure ratio becomes erratic and finally decreases below the initial constant value. This behavior

is attributed to the effects of reservoir contamination - the mixing of driver gas, mostly helium, with test gas in the reservoir. A pressure decrease is expected because the effective isentropic index of the test gas is raised as a result of its dilution with driver gas. For example, the static pressure is decreased by almost an order of magnitude in an expansion when pure driver gas is used.

Pitot pressure.- Two pitot-pressure histories, normalized with respect to the reservoir pressure, are shown in figure 6(b). Notice that in one case the pitot-pressure record indicates quasi-steady flow during the first 8 msec of the flow time, while in the other, the time interval is about 14 msec. These different time intervals illustrate the well known fact that test time can vary significantly from run to run in shock-driven facilities, particularly in overtailored operation. Such behavior is usually attributed to differences in interface mixing brought about by relatively minor variations in the mechanics of opening the main diaphragm. The times illustrated here are characteristic of this facility at this operating condition; a similar range of times was observed for other measurements in the test section.

The pitot-pressure level is approximately constant, and at the level shown in figure 6(b), across an 18-cm-diameter core of the test-section flow. This indicates that the flow is free of interference from boundary-layer effects in this core. Pitot-pressure measurements obtained at an axial position about 10 cm downstream of the nominal test station indicate an axial Mach number gradient of about 0.016 per cm due to conical flow expansion.

Tests with several multiple probe configurations have shown that there is no appreciable change in the effective area ratio of the flow, due to the presence of the probes in the stream.

Mass flow.- The mass-flow rate per unit area, normalized with the reservoir pressure, is shown in figure 6(c) for $p_i = 0.34$ atm. Notice that a significant time interval is required to establish steady-state operation. Recall that this transient is due to the filling process of the mass-flow probe itself, rather than to the flow starting process (unsteady wave system) in the shock-tunnel nozzle.

The unit mass-flow rate has a slight dependence on the reservoir enthalpy. This dependence is negligible for the enthalpy variations shown in figure 4(b). Also, since the temperature rose only 6° C in the probe cavity during this run, the correction to the mass flow for this effect is very small.

Free-stream velocity.- The free-stream velocity measured for $p_i = 0.34$ atm is shown in figure 6(d), normalized with respect to the limiting velocity, considering an equilibrium expansion with the same initial conditions. For this particular loading pressure, the velocity ratio is relatively insensitive, with time, to driver-gas contamination, since the total enthalpy of the driver gas behind the reflected shock wave is approximately equal to the total enthalpy of the test gas. However, the two data points at 22 and 23 msec from diaphragm rupture denote a small change in flow velocity, which is probably due to the onset of contamination.

The chief merit of this probe as a diagnostic tool is that the free-stream velocity is essentially independent of the effective area ratio of the nozzle for the highly expanded flows considered here. Thus, in the absence of other energy losses, the magnitude of the free-stream velocity provides a measure of the amount of energy frozen chemically and vibrationally.

ANALYSIS OF RESULTS

The experimental data presented in the preceding section are analyzed in this section using two models for the nonequilibrium, chemically and vibrationally relaxing gas. The purpose of this analysis is to determine the remaining aerodynamic properties of the free stream.

Flow Models

Numerical calculations which couple the quasi-one-dimensional gas-dynamic equations with chemical and vibrational rate equations conceptually yield exact solutions for nozzle flow properties. Typical numerical solutions for nonequilibrium airflows are presented in references 10 and 11. One difficulty with the application of numerical techniques is the choice of the appropriate rate constants and/or relaxation mechanisms. For example, discrepancies between the results of such calculations and measurements for air have been attributed to uncertainties in vibrational relaxation of nitrogen (refs. 12 and 13).

The effective sudden freeze concept outlined in appendix A provides a mathematical model for nonequilibrium flow in a nozzle that predicts certain aerodynamic properties of the free stream without knowledge of the precise relaxation process or corresponding rate constants. This technique assumes that most properties of the gas in the test section, having undergone relaxation of several internal degrees of freedom, are approximately the same as though the gas instantaneously had made a transition from full equilibrium flow to flow in which all internal energy exchange is frozen. In one-dimensional flow this process can then be characterized by a single parameter, the Mach number of transition to internally frozen flow, where the Mach number is for equilibrium sound speed and constant entropy.

Static pressure as a function of pitot pressure is shown in figures 7(a) through (c). The normalized static pressure is plotted as a function of the corresponding normalized pitot pressure in figure 7(b) for the nozzle expansion with $p_i = 0.34$ atm. Curves of static pressure versus pitot pressure, calculated according to the sudden-freeze technique, are shown in the figure (solid-line curves) with area ratio and effective-freeze Mach number as parameters. Curves of static pressure versus pitot pressure, calculated using the numerical procedure of reference 11, are also shown (dashed-line curves). One of these curves is obtained assuming complete equilibrium, that is, both the chemistry and the vibrational energy modes are computed assuming infinite rate constants; another curve is computed assuming that the

chemistry is in nonequilibrium and the vibrational mode is in equilibrium; and the last is computed assuming both chemical and vibrational (uncoupled) nonequilibrium. The rate parameters used for the nonequilibrium calculations are commonly accepted parameters (ref. 11 or 15) and were obtained originally from shock-tube data.

It will be observed that the experimental data lie between the curves for vibrational equilibrium and nonequilibrium. This result could imply that the effective vibrational relaxation times used for the nonequilibrium calculations, as obtained from shock-tube data, are too large for the expanding flow - an implication that is consistent with the findings of other researchers (refs. 16 through 19). In a more general sense, however, the present result probably should not be interpreted as due solely to a defect in vibrational relaxation times. Rather, it should also be recognized that the relaxation mechanisms used may not be correct. For example, vibration-dissociation coupling may well be important in this application. For this reason, then, the model of reference 11 has been used only to indicate approximate boundaries for the relaxation processes. A more exact delineation of mechanisms or rates is beyond the scope of the present report.

For all the curves plotted in figure 7(b), the pitot pressure was calculated assuming that both the vibrational energy mode and the chemistry were frozen along the stagnation streamline behind the standing shock wave. This assumption is realistic for the flow conditions and probe size used in this study.

Notice that a simultaneous determination of pitot and static pressure will uniquely fix the area ratio, the freeze Mach number, and hence all other flow variables, according to the effective sudden-freeze concept. Measurements such as these could be useful for resolving uncertainties in relaxation mechanisms or rates in expanding flows in a carefully controlled experiment.

Data Analysis

The aerodynamic properties of the test stream for $p_i = 0.34$ atm can be determined by correlating the pitot- and static-pressure measurements with the sudden-freeze calculations shown in figure 7(b). The intersection of the pitot- and static-pressure ratios defines an effective freeze Mach number and the area ratio for the flow. Knowing the area ratio and effective-freeze Mach number, all other flow properties can be calculated according to the sudden-freeze technique. The results of these calculations for the conditions of figure 7(b) are shown in table I(b). These results represent the aerodynamic calibration of the test stream for $p_i = 0.34$ atm within the accuracies indicated in appendix A. Notice that the independent measurements of mass flow and velocity, which are redundant measurements according to this application of the sudden-freeze technique, are in good agreement with mass flow and velocity derived from the sudden-freeze calculation.

Carpet plots similar to that in figure 7(b) are shown in figures 7(a) and (c) for $p_i = 0.54$ and 0.25 atm, respectively. The aerodynamic calibrations of the test stream for these conditions are shown in tables I(a) and I(c), respectively.

Average test duration results are also shown for each of the three operating conditions in tables I(a), I(b), and I(c). Relatively long contamination-free test times were obtained at the nominal tailored-interface (p_i = 0.34 atm) and the undertailored (p_i = 0.54 atm) operating conditions. The test time is substantially less for the overtailored case (p_i = 0.25 atm). As anticipated from the results of other investigators (e.g., ref. 20), preliminary measurements indicate that the test times become even shorter as the initial driven-tube loading pressure is decreased further. Test times of considerably longer and shorter durations than the "most likely" values in these tables have been observed at each of these test conditions. For this reason, it has been found advisable to monitor the flow during each test with some device (e.g., a pitot-pressure probe) that is sensitive to changes in flow properties.

Some of the aerodynamic properties of shock-tunnel test streams can be found by the techniques presented in this report, even if the test gas is diluted with driver gas. Appendix B shows how the useful test duration of the shock tunnel can be extended by testing in slightly contaminated test gas. The degree to which this can be done depends, of course, on which parameters are significant for the individual simulation problem at hand.

CONCLUDING REMARKS

An analysis and the results of a preliminary calibration of the nonequilibrium test stream in the Ames 1-foot shock tunnel are presented for reservoir enthalpies of 7,600, 9,100, and 10,900 J/gm at a nominal reservoir pressure of 275 atm. The test gas in the reservoir is in local thermodynamic equilibrium and is free of significant radiation and conduction heat losses.

The free-stream flow in the test section is affected by both chemical and vibrational nonequilibrium, and the data obtained are within an order of accuracy consistent with the present uncertainty of the relaxation mechanisms and/or rates. It was found that a semiempirical, sudden-freeze model is satisfactory for determining test stream properties and that such an approach is convenient since the results are not dependent on any specification of rates.

The average duration of the test gas flow was found to be limited by the onset of contamination by driver gas and varied from about 15 msec at a reservoir enthalpy of 7,600 J/gm to about 4 msec at a reservoir enthalpy of 10,900 J/gm.

Ames Research Center
National Aeronautics and Space Administration
Moffett Field, Calif. 94035 Sept. 13, 1968
129-01-08-10-00-21

APPENDIX A

SEMIEMPIRICAL SUDDEN-FREEZE MODEL

Consider a nonequilibrium expansion of high-temperature air in a nozzle. Now consider two numerical-rate calculations for this expansion, neither of which necessarily represents the real expansion because of uncertainties in either relaxation processes or times. The present sudden-freeze technique is based on the following hypothesis: a sudden-freeze solution, characterized by a freeze Mach number, can be found that accurately represents each of these numerical solutions at large area ratios, A/A^*, far downstream of the relaxation region.

This will be demonstrated by examining the calculations presented in table II. Two "exact" numerical calculations differing only in the value of the vibrational relaxation time of N_2 are shown for a particular expansion. The two matching sudden-freeze solutions (simultaneous freezing of chemistry and vibrations), each characterized by an effective-freeze Mach number, are also shown. Notice that the aerodynamic parameters calculated according to sudden-freeze concepts match the corresponding parameters calculated numerically within a few percent in both cases. Similar results have been observed for a variety of reservoir conditions and nozzle area ratios, with air as the nonequilibrium expanding gas. It is recognized of course that parameters such as vibrational temperature and chemical composition, that depend on the distribution of internal energy in the frozen degrees of freedom, cannot be matched in this manner.

Therefore, a conclusion can be drawn: a sudden-freeze solution exists that accurately duplicates, at large area ratios, the aerodynamic properties obtained from numerical calculations of a nonequilibrium air expansion. (This includes the numerical solution that exactly represents the real expansion.) Hence, if one is calculating aerodynamic properties of nonequilibrium nozzle flows for which the relaxation mechanisms are uncertain it is preferable to use the sudden-freeze solution that matches the real flow rather than a numerical solution with uncertain rate constants.

The obvious difficulty with using the effective-freeze concept is the determination of the particular sudden-freeze solution that duplicates the correct, but unknown, numerical solution to an expansion. Fortunately the effective-freeze Mach number that corresponds to the real flow can be found by making two independent measurements in the free stream. Hayman (ref. 14) points out a convenient method of finding the freeze Mach number and area ratio of a nonequilibrium air flow using two free-stream measurements. His technique is used in the present text to determine the effective-freeze Mach numbers for the nonequilibrium streams examined here. A prerequisite for applying any of these models is knowing the reservoir conditions. Reservoir pressure can usually be measured, while reservoir enthalpy can be computed from incident and reflected-shock properties and verified by free-stream heat-transfer measurements.

As mentioned previously, the effective-freeze approach probably cannot be used to determine properties such as chemical composition and vibrational temperature — properties that are directly related to the internal energy distributions in the nonequilibrium degrees of freedom. Therefore, if the specification of these parameters is required for proper simulation of an experiment, the effective-freeze method may not be adequate, and it may be necessary to apply experimental techniques, such as spectroscopic analyses, to measure the required internal energy distribution of the gas.

APPENDIX B

INFLUENCE OF CONTAMINATION ON STREAM CALIBRATION

It has been found desirable on occasion to operate the 1-foot shock tunnel at high-enthalpy, overtailored conditions for which it is likely that the reservoir gas is quickly contaminated with driver gas. It will be shown in this appendix that useful data can be obtained after the onset of driver gas contamination at standard operating conditions, such as discussed in the text, and that aerodynamic properties of streams with unknown amounts of driver gas contamination can be approximated by utilizing only pure-air nozzle calculations. It will be simply demonstrated, for conditions of interest in the 1-foot shock tunnel, that sudden-freeze nozzle calculations for pure air and air-helium mixtures yield approximately the same stream properties when based on pitot- and static-pressure measurements. The air-helium mixture is a reasonable substitution for the actual air-driver gas mixture of interest and provides a considerable simplification.

Consider sudden-freeze calculations, similar to those in the text, for a nozzle flow of pure air and an air-helium mixture consisting of 25-percent helium by mole fraction. This relatively large amount of helium was arbitrarily chosen for illustration purposes and does not imply actual contamination levels. For this discussion, consider a reservoir enthalpy of 10,900 J/gm and a reservoir pressure of 275 atm for both cases. These values correspond to the p_i = 0.25-atm loading condition discussed in the text, both before and after the onset of contamination in the reservoir.

The particular sudden-freeze solution corresponding to the measured pitot and static pressure is shown in table III for each reservoir gas. These pressures are obtained after the onset of contamination, approximately 10 msec from the beginning of flow in the nozzle; note that they are not the same as measured earlier in the test (table I(c)). It will be observed that the freeze Mach numbers and the area ratios derived for the two cases are different. Comparing the flow Mach numbers, temperatures, velocities, densities, and dynamic pressures, it is apparent that the two solutions yield approximately the same results for these aerodynamic properties. It is also seen that the free-stream Reynolds numbers are approximately equal for the two cases since the viscosities of the two gas mixtures, according to reference 21, are nearly equivalent at the same temperature.

Results similar to those in the table have been obtained when air-helium mixtures with smaller helium proportions are compared with pure-air results. Therefore, it is seen that pure-air sudden-freeze calculations are adequate for deriving approximations to aerodynamic properties such as Mach number and Reynolds number for streams contaminated with relatively large amounts of helium. This result indicates the effects encountered when the air test gas in the 1-foot shock tunnel becomes contaminated with the combustion-heated driver gas used in the facility. The results for pure air in table III have been used as an approximate stream calibration for the p_i = 0.25-atm loading condition of the 1-foot shock tunnel, at times from 10 to 30 msec after the start of flow.

REFERENCES

1. Cunningham, Bernard E.; and Kraus, Samuel: A 1-Foot Hypervelocity Shock Tunnel in Which High-Enthalpy Real-Gas Air Flows Can Be Generated With Flow Times of About 180 Milliseconds. NASA TN D-1428, 1962.

2. Loubsky, William J.; Hiers, Robert S.; and Stewart, David A.: Performance of a Combustion Driven Shock Tunnel With Application to the Tailored-Interface Operating Conditions. Paper presented at the Third Conference on the Performance of High Temperature Systems, Pasadena, December 1964.

3. Holder, D. W.; and Schultz, D. L.: On the Flow in a Reflected Shock Tunnel. Aeronautical Research Council (Gt. Brit.). National Phys. Lab., London, HMSO, 1962 (previously issued as ARC 22152).

4. Dannenberg, Robert E.; and Stewart, David A.: Technique for Improving the Opening of the Main Diaphragm in a Large Combustion Driver. NASA TN D-2735, 1965.

5. Bowman, Gary H.; and Coon, Grant W.: Static Pressure Measurements in a Hypervelocity Shock Tunnel. AIAA J., vol. 3, no. 4, April 1965, pp. 751-752.

6. Brown, Alan C.; Kramer, Raymond L.; McAdams, Edward E., Jr.; and Smith, C. Edward, Jr.: The Use of Mass-Flow and Total Enthalpy Probes in Supersonic Flow. IEEE Proc., First International Congress on Instrumentation in Aerospace Simulation Facilities, Paris, France, 1964. (TR B-07-64-1, Lockheed Missiles and Space Co., Palo Alto, Calif., September 1964).

7. Kyser, James B.: A Study of the Structure of Spark Columns for Velocity Measurements in a Hypersonic Stream. SUDAAR No. 272, June 1966.

8. Hiers, Robert S., Jr.; and Loubsky, William J.: Effects of Shock Wave Impingement on the Heat Transfer on a Cylindrical Leading Edge. NASA TN D-3859, 1967.

9. Fay, J. A.; and Riddell, F. R.: Theory of Stagnation Point Heat Transfer in Dissociated Air. J. Aero. Sci., vol. 25, no. 2, February 1958, pp. 73-85 and 121.

10. Lordi, J. A.; and Mates, R. E.: Nonequilibrium Effects on High-Enthalpy Expansions of Air. AIAA J., vol. 3, no. 10, October 1965, pp. 1972-1974.

11. Reinhardt, Walter A.; and Baldwin, Barrett S., Jr: A Model for Chemically Reacting Nitrogen-Oxygen Mixtures With Application to Non-equilibrium Air Flow. NASA TN D-2971, 1965.

12. Hurle, I. R.; Russo, A. L.; and Hall, J. Gordon: Experimental Studies of Vibrational and Dissociative Nonequilibrium in Expanded Gas Flows. Preprint 63-439, AIAA, Aug. 26-28, 1963.

13. Nagamatsu, H. T.; and Sheer, R. E., Jr.: Vibrational Relaxation and Recombination of Nitrogen and Air in Hypersonic Nozzle Flows. AIAA J., vol. 3, no. 8, Aug. 1965, pp. 1386-1391.

14. Hayman, Lovick O., Jr.; and Stewart, Roger B.: A Technique for Determining the Nozzle-Flow Properties of Air in an Equilibrium, Nonequilibrium, or Frozen State. J. Aero. Sci., vol. 29, no. 2, 1963, p. 245.

15. Garr, Leonard, Jr.; and Marrone, Paul V.: Inviscid, Nonequilibrium Flow Behind Bow and Normal Shock Waves, Part II. The IBM 704 Computer Programs. Cornell Aero. Lab. Rep. QM-1626-A-12 (II), May 1963.

16. Sebacher, Daniel I.: A Correlation of N_2 Vibrational → Translational Relaxation Times. AIAA J., vol. 5, no. 4, April 1967, pp. 819-820.

17. Fishburne, E. S.; Petrie, S. L.; and Pierce, G. A.: Analysis of the Thermo-Chemical State of an Expanded Air Plasma. Final Report Air Force Flight Development Center, AFFDL TR-64-191, Aug. 1965.

18. Tirumalesa, Duvvuri: Nozzle Flows with Coupled Vibrational and Dissociational Nonequilibrium. AIAA J., vol. 5, no. 2, Feb. 1967, pp. 254-260.

19. Hall, J. G., and Russo, A. L.: Recent Studies of Nonequilibrium Flows at the Cornell Aeronautical Laboratory. AGARD CP No. 12, vol. 2, pt. III, 1967, pp. 443-476.

20. Kaegi, E. M.; and Muntz, E. P.: Driver-Driven Gas Mixing and Its Effect on Shock Tunnel Test Time. Third Hypervelocity Techniques Symposium, Denver, Colorado, March 1964.

21. Eckert, E. R. G.; Ibele, W. E.; and Irvine, T. F., Jr.: Prandtl Number, Thermal Conductivity, and Viscosity of Air-Helium Mixtures. NASA TN D-533, 1960.

TABLE I.- SUMMARY OF CALIBRATION RESULTS

Free-stream property	Experimental value	Derived value
(a) p_t = 275 atm, h_t = 7600 J/gm, p_i = 0.54 atm		
A/A^* $(=\rho^*u^*/\rho u)$	3600	3470
M_f	- - -	3.3
p/p_t	2.50×10^{-6}	2.50×10^{-6}
p_{t_2}/p_t	5.30×10^{-4}	5.30×10^{-4}
ρ/ρ_t	- - -	8.90×10^{-5}
T/T_t	- - -	4.28×10^{-2}
u/u_{max}	0.96	0.96
Re/p_t, 1/cm atm	- - -	11.1
M	- - -	12.6
Avg. test duration	15 msec	- - -
(b) p_t = 275 atm, h_t = 9100 J/gm, p_i = 0.34 atm		
A/A^* $(=\rho^*u^*/\rho u)$	3300	3410
M_f	- - -	3.8
p/p_t	3.03×10^{-6}	3.03×10^{-6}
p_{t_2}/p_t	5.40×10^{-4}	5.40×10^{-4}
ρ/ρ_t	- - -	6.30×10^{-5}
T/T_t	- - -	5.33×10^{-2}
u/u_{max}	0.95	0.96
Re/p_t, 1/cm atm	- - -	7.94
M	- - -	11.6
Avg. test duration	9 msec	- - -
(c) p_t = 275 atm, h_t = 10,900 J/gm, p_i = 0.25 atm		
A/A^* $(=\rho^*u^*/\rho u)$	- - -	3560
M_f	- - -	3.9
p/p_t	2.90×10^{-6}	2.90×10^{-6}
p_{t_2}/p_t	5.15×10^{-4}	5.15×10^{-4}
ρ/ρ_t	- - -	5.95×10^{-5}
T/T_t	- - -	5.55×10^{-2}
u/u_{max}	0.95	0.96
Re/p_t, 1/cm atm	- - -	6.54
M	- - -	11.7
Avg. test duration	4 msec	- - -

TABLE II.- COMPARISON OF NUMERICAL AND MATCHING SUDDEN-FREEZE SOLUTION FOR h_t = 9100 J/gm, p_t = 275 atm

Free-stream property	Nonequilibrium vibrations		Equilibrium vibrations	
	Numerical solution	Sudden-freeze solution	Numerical solution	Sudden-freeze solution
A/A^*	3000	3000	3000	3000
M_f	- - -	3.3	- - -	4.4
p/p_t	3.09×10^{-6}	3.09×10^{-6}	4.16×10^{-6}	4.16×10^{-6}
ρ/ρ_t	7.25×10^{-5}	7.25×10^{-5}	7.07×10^{-5}	7.01×10^{-5}
T/T_t	4.69×10^{-2}	4.63×10^{-2}	6.44×10^{-2}	6.50×10^{-2}
u, cm/sec	4.05×10^{5}	4.04×10^{5}	4.13×10^{5}	4.10×10^{5}

TABLE III.- INFLUENCE OF RESERVOIR COMPOSITION ON FREE-STREAM PROPERTIES

	h_t = 10,900 J/gm, p_t = 275 atm	
	100% Air	75% Air, 25% He
p/p_t	1.9×10^{-6}	1.9×10^{-6}
p_{t_2}/p_t	4.9×10^{-4}	4.9×10^{-4}
M_f	2.5	3.0
A/A^*	3450	3650
u, m/sec	4100	4400
T, ^oK	190	190
ρ, g/cm^3	0.90×10^{-6}	0.78×10^{-6}
M	14	14
q/p_t	2.7×10^{-4}	2.6×10^{-4}
Re, 1/cm	2900	2650

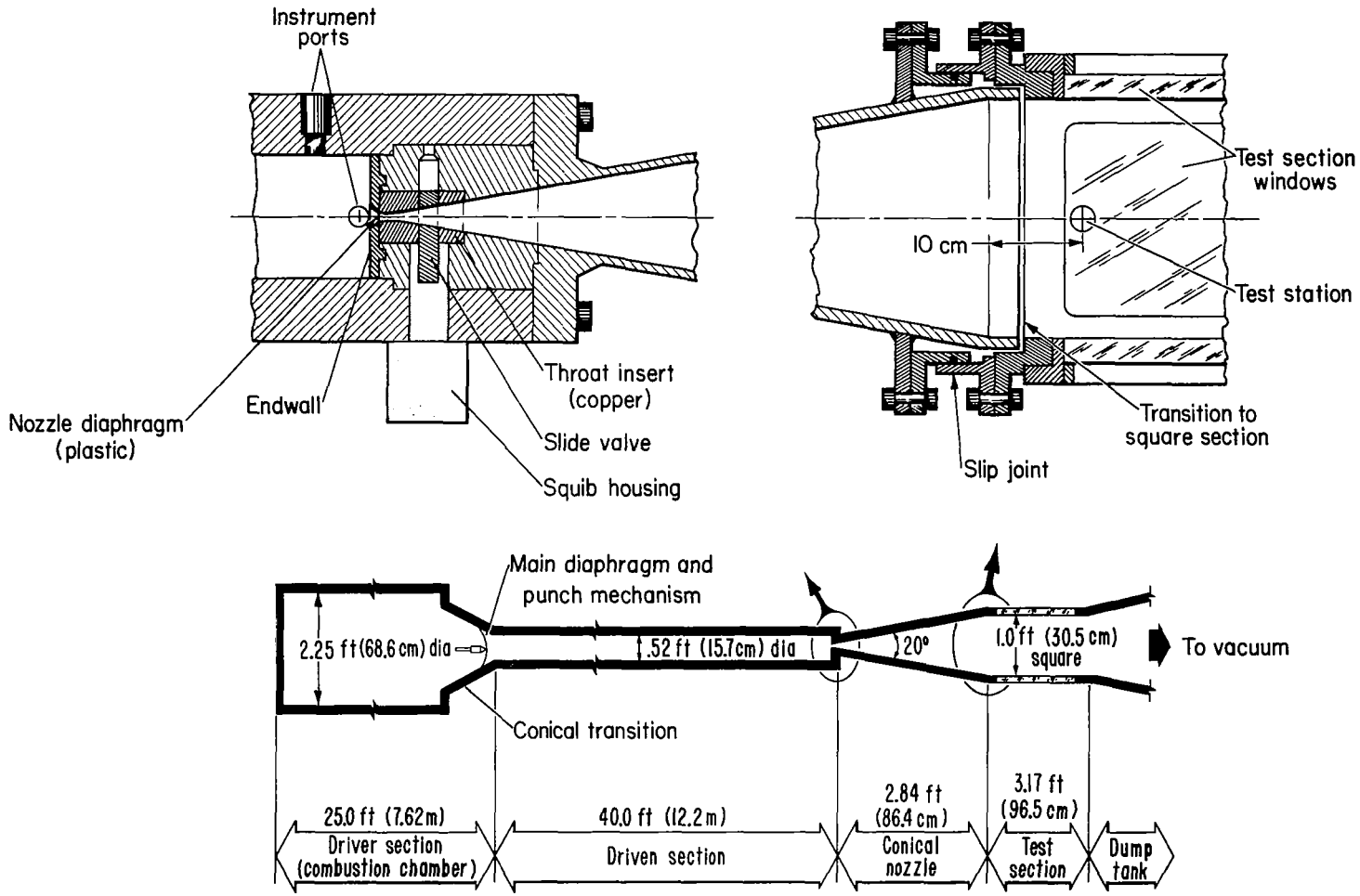

Figure 1.- Schematic drawing of the Ames 1-foot shock tunnel with nozzle assembly details.

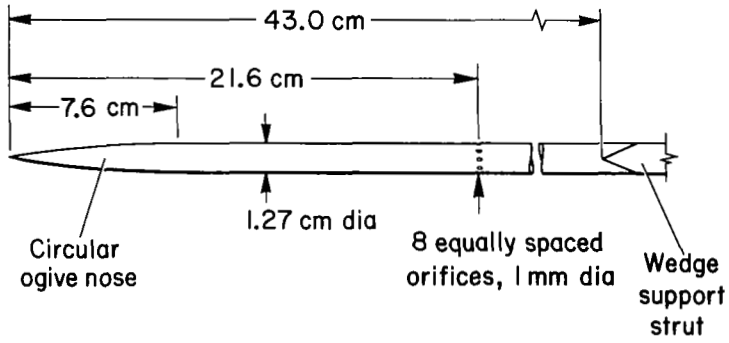

(a) Static-pressure probe.

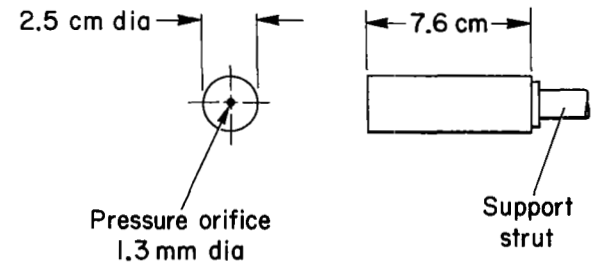

(b) Pitot-pressure probe.

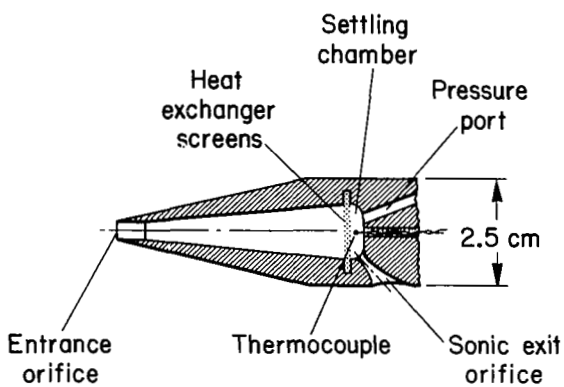

(c) Mass-flow probe.

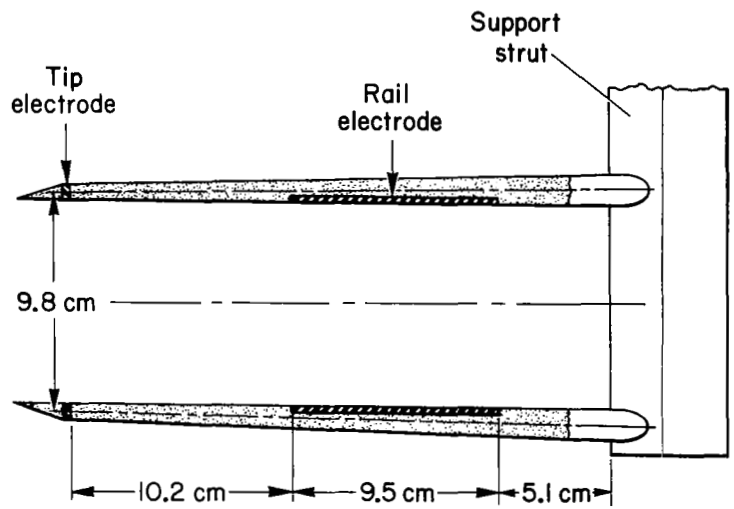

(d) Velocity probe.

Figure 2.- Test-section instrumentation.

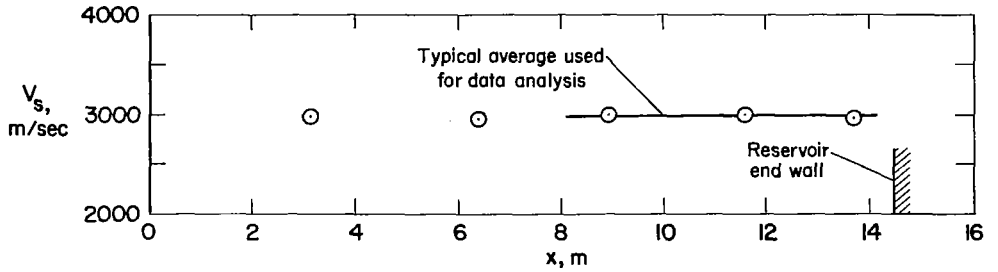

Figure 3.- Incident shock velocity in driven tube; p_i = 0.34 atm.

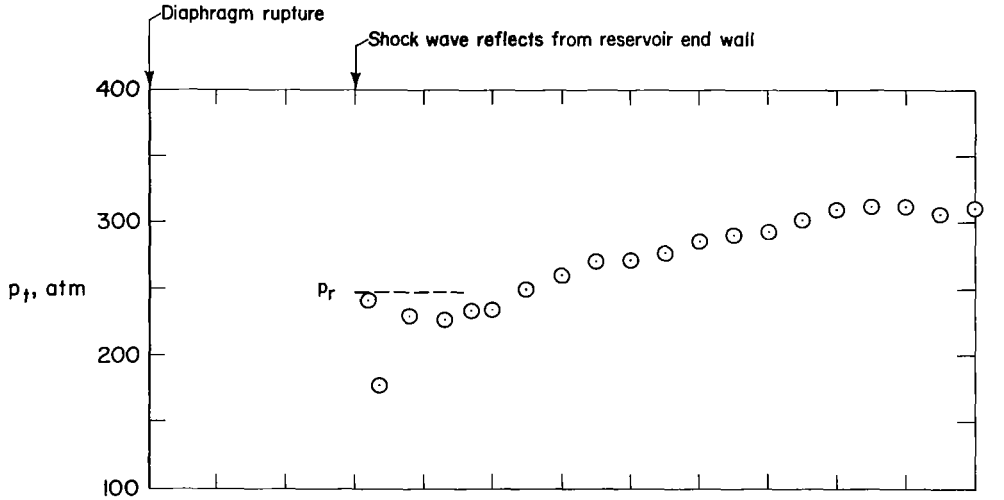

(a) Pressure.

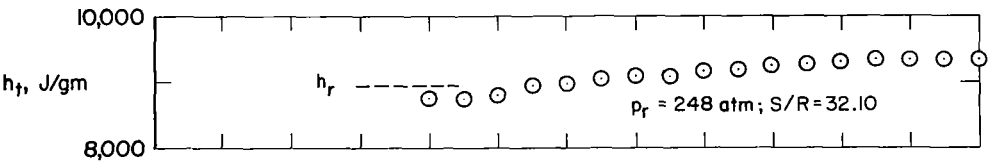

(b) Enthalpy.

Figure 4.- History of reservoir conditions; p_i = 0.34 atm.

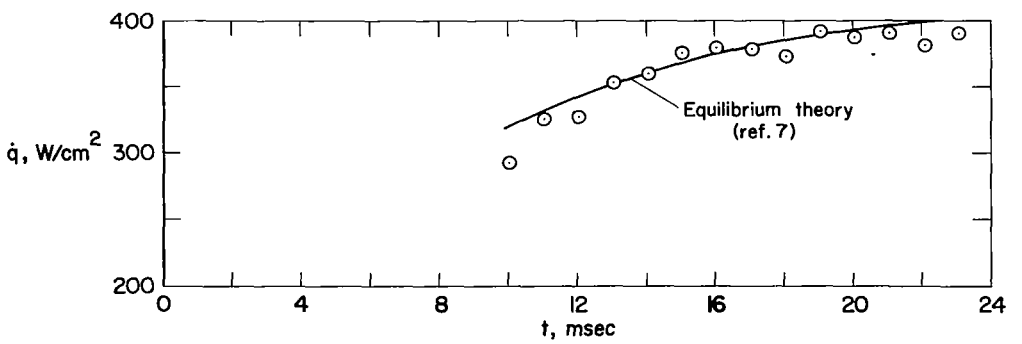

Figure 5.- Heat-transfer rate to stagnation point of 2.5-cm hemisphere; p_i = 0.34 atm.

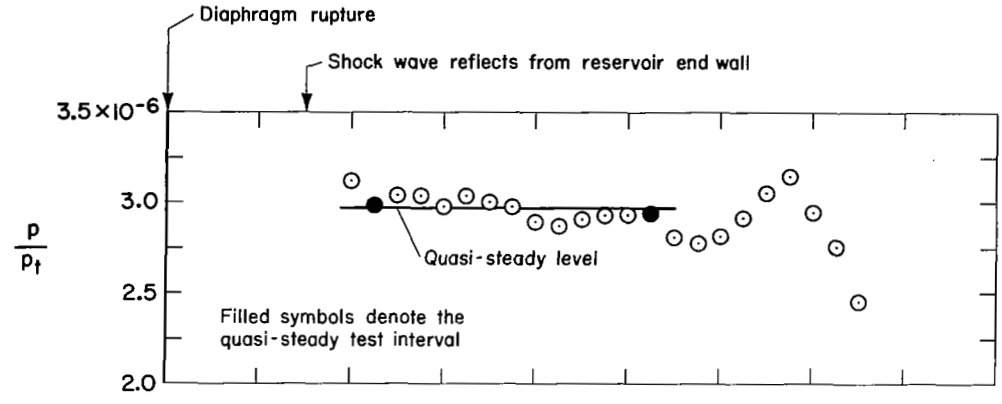

(a) Static-pressure ratio.

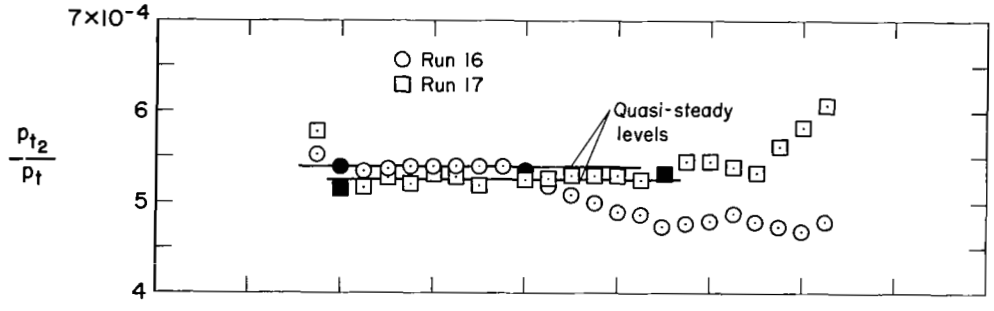

(b) Pitot-pressure ratio.

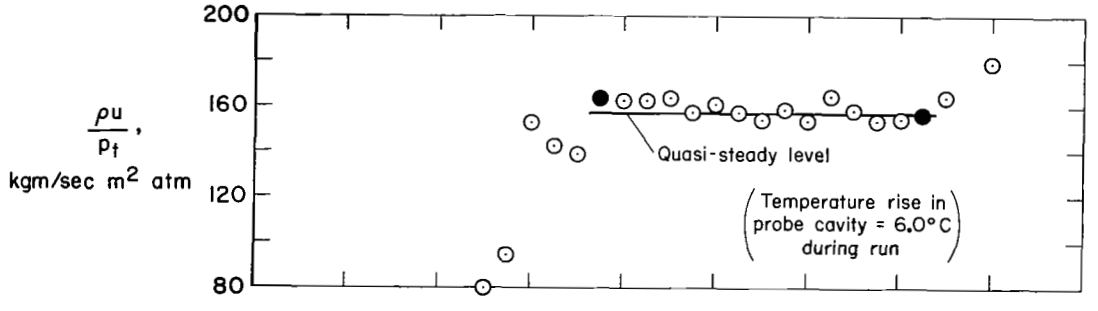

(c) Mass-flow parameter.

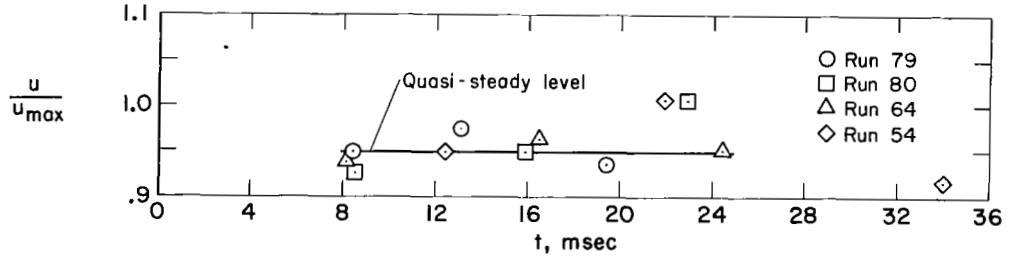

(d) Velocity ratio.

Figure 6.- Free-stream conditions; p_i = 0.34 atm.

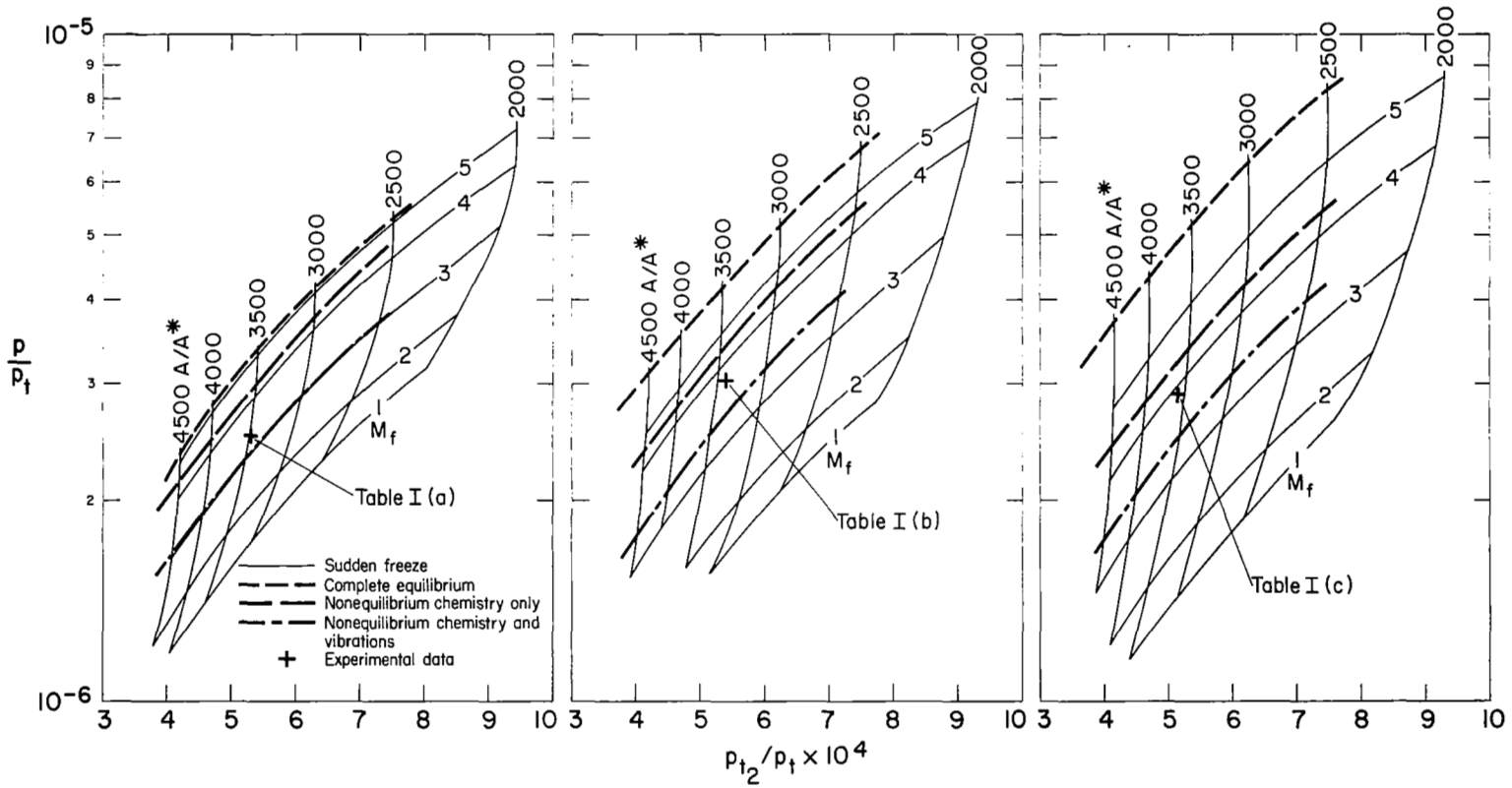

(a) p_i = 0.54 atm; h_t = 7600 J/g

(b) p_i = 0.34 atm; h_t = 9100 J/g

(c) p_i = 0.25 atm; h_t = 10,900 J/g

Figure 7.- Comparison of measured stream pressures with sudden-freeze results and numerical solutions.